Research on the Blades and Performance of Semi-Submersible Wind Turbines with Different Capacities

Jiaping Cui [1], Zhigang Cao [2], Pin Lyu [2], Huaiwu Peng [3], Quankun Li [1], Ruixian Ma [1,*] and Yingming Liu [4]

1 School of Power and Energy, Northwestern Polytechnical University, Xi'an 710129, China; cuijiaping2024@163.com (J.C.)
2 Goldwind Science & Technology Co., Ltd., Urumqi 830026, China
3 Power China Northwest Engineering Co., Ltd., Xi'an 710065, China
4 School of Electrical Engineering, Shenyang University of Technology, Shenyang 110870, China
* Correspondence: maruixian@nwpu.edu.cn

Abstract: With the gradual increase in the maturity of wind energy technology, floating offshore wind turbines have progressively moved from small-capacity demonstrations to large-capacity commercial applications. As a direct component of wind turbines used to capture wind energy, an increase in the blade length directly leads to an increase in blade flexibility and a decrease in aerodynamic performance. Furthermore, if the floater has an additional six degrees of freedom, the movement and load of the blade under the combined action of wind and waves are more complicated. In this work, two types of semi-submersible wind turbines with different capacities are used as the research objects, and the load and motion characteristics of the blades of these floating offshore wind turbines are studied. Through the analysis of the simulation data, the following conclusions are drawn: with the increase in the capacity of the wind turbine, the flexible deformation of the blade increases, the movement range of the blade tip becomes larger, the blade root load increases, and the power fluctuation is more obvious. Compared with the bottom-fixed wind turbine, the flexible blade deformation of the floating offshore wind turbine is smaller; however, the blade root load is more dispersed, and the power output is more unstable and lower.

Keywords: floating wind turbine; blade root load; flexible deformation; power output

1. Introduction

With the increasing demand for wind power around the world, wind turbines have gradually developed toward the deep sea, and floating offshore wind turbines (FOWTs) have emerged to address the current requirements [1]. Due to the additional six degrees of freedom (DOFs) of FOWTs, the blades and other components have a larger range of motion under the combined action of wind and waves than in bottom-fixed offshore wind turbines [2]. In addition, offshore wind is more stable and the average wind speed is higher, so the capacity of offshore wind turbines, especially FOWTs, is very large. Most of the FOWTs in commercial operation will have a capacity greater than 10 MW in the future [3,4]. A greater capacity means an increase in the size, volume, and mass of the wind turbine components.

As the main components of wind turbines used to capture wind energy, the characteristics of the blades during operation are critical to the efficiency of wind energy capture [5]. With an increase in the blade's length, its stiffness decreases and its flexibility increases, which leads to a reduction in the swept area of the rotor and affects the power output of the wind turbine. The tilting of the FOWT can also have a influence on the rotor's swept aera. In addition, an increase in blade flexibility also increases the range of motion of the blade tip, which will increase the occurrence of strike events between the tower and blade; this needs to be solved by increasing the blade cone angle [6]. For the blades of FOWTs, the

movement of the floating platform is coupled with the blade movement, resulting in larger and more complex blade movement [7].

Many experts and scholars throughout the world have studied the aerodynamic characteristics and blade loads of floating wind turbines. Lienard C. studied the aerodynamics of a floating offshore wind turbine standing on a Spar floater, considering several types of motion to describe the wind turbine, both representative of the floating behavior and simple to implement [8]. Youngjin Kim and Oh Joon Kwon conducted research on the effect of platform motion on the aerodynamic performance and aeroelastic behavior of floating offshore wind turbine blades. It was found that the load variation caused by the platform surge or pitch motion had a significant influence on the flapwise and torsional deformations of the rotor blades [9]. Juchuan Dai et al. studied the load and dynamic characteristics of wind turbines' flexible blades. They considered the influence of the electrical system, and the blade vibration speed experienced a large change when coupled with the electromagnetic torque of the generator [10]. Bozzo performed a dynamic analysis of floating offshore wind turbines under extreme operational conditions; an analysis of the average and maximum design load case stress conditions was performed, followed by a fatigue analysis using the IEA-15MW wind turbine [11]. Yu Z studied a hybrid numerical model for the simulation of the aero-elastic-hydro-mooring-wake dynamic responses of a floating offshore wind turbine, and this model showed good agreement with the results from other methods [12]. Liang G et al. performed an experimental investigation of two shared mooring configurations for a dual-spar floating offshore wind farm in irregular waves [13]. Wang K used an artificial-neural-network-based method to predict the extreme responses of floating offshore wind turbines under operating conditions [14]. These scholars have studied the blade characteristics, power output, and loads of floating wind turbines either by simulation or by experiments. However, few studies have examined the load, motion, and power fluctuation characteristics associated with floating and fixed wind turbines of the same capacity, as well as wind turbines having same type of foundation but different capacities.

There are three mainstream types of floating platforms in practical engineering applications, and the concepts of the three types of FOWTs are shown in Figure 1. The semi-submersible (semi) model consists of a main column connected to the tower and three offset columns connected to the main column. The catenary of the mooring system is connected near the bottom of each offset column. The floating foundation of this design is relatively large in volume and weight [15]. The spar buoy (spar) is a platform that has three notable features: a very deep draft, a long and thin spar buoy, and three catenary lines. The three catenaries are usually distributed in triangles to increase the yaw stiffness of the floating platform [16]. The tension leg platform (TLP) is a platform whose main structure is a cylindrical platform; the ballast tank is filled with concrete, and the mooring system consists of four pairs of vertical steel bars. The concrete ballast and the mooring system jointly ensure the stability of the floating platform. Even when there is no mooring system, the platform can remain stable within a certain range [17].

Semi-submersible platforms are usually composed of multiple large columns connected by diagonal braces. At present, three-column and four-column foundations are more common. The wind turbine can be installed on any column, and the larger water surface area of the column is used to ensure the stability of the wind turbine. The ballast inside the column is used to adjust the overall center of gravity and buoyancy of the wind turbine [18,19]. In addition, the semi-submersible platform usually consists of three triangularly distributed catenary lines to improve the yaw stiffness of the wind turbine. Due to their advantages of convenient installation, convenient operation and maintenance, good stability, and reliable operation, most floating wind plants currently under construction or in planning use semi foundations as floating platforms for wind turbines [20]. In particular, the most used floating platform among the three types of floaters in engineering applications is the semi, so we select the semi-type floating platform as the object of our research.
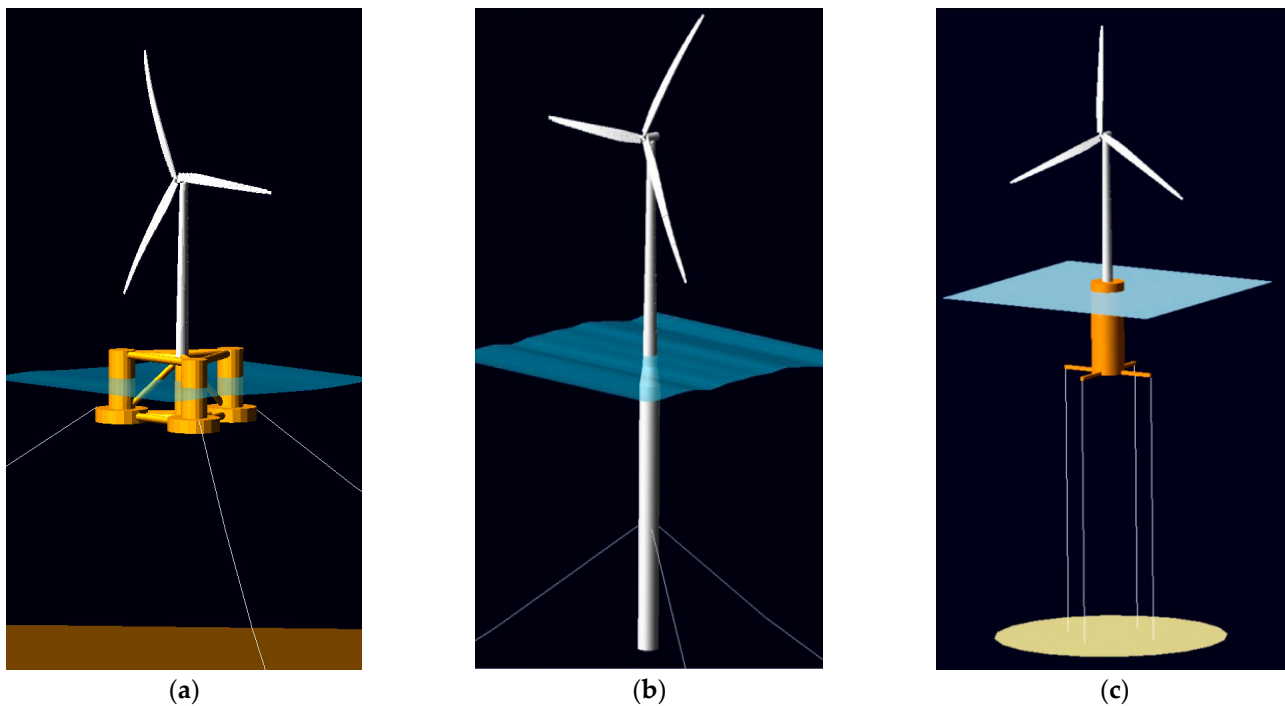
Figure 1. Concepts of three types of floating wind turbines: (**a**) semi, (**b**) spar, (**c**) TLP.

On the basis of the above research, this paper focuses on the blade's load and motion characteristics in semi-type wind turbines with different capacities, as well as the differences in the power output of wind turbines with different platforms. The second section presents the methodology for the simulation, as well as the model parameters of the semi-submersible floating platform and wind turbines, including NREL-5MW and IEA-15MW. The third section introduces the case conditions, which includes the wind conditions, wave conditions, and case studies. The fourth section analyzes the simulation results and presents a discussion from the perspectives of rotor motion, blade tip motion, the clearance between the tower and blade, the power output, etc. Section 5 gives the conclusions.

2. Methodology and Models

2.1. Methodology and OpenFAST Model

The main methodology is that using the time domain analysis tool OpenFAST 3.0.0, developed by NREL, to investigate the blade characteristics and performance of the NREL-5MW and IEA-15MW semi-type FOWTs and a monopile-type bottom-fixed wind turbine in various wind and wave environments [21]. At the same time, we use the high-fidelity method to calculate the dynamics, for which we select BeamDyn in OpenFAST. A diagram of methodology is shown in Figure 2. Firstly, the wind and wave conditions, as well as the model parameters of the wind turbine and floating platform, need to be selected and set. Then, OpenFAST begins a simulation using these conditions and parameters as inputs. OpenFAST can calculate the rotor dynamics, platform dynamics, mooring dynamics, and so on. Through these calculations, the series data of the output parameters, such as the power output, blade load, and blade motion, can be obtained.

The system mainly includes an aerodynamic module, hydrodynamic module, anchor chain module, and control module. The dynamic equation of the whole system can be expressed as

$$[M(s) + M(a) + M_{WT}]\ddot{x} + [C(s) + C_{WT}]\dot{x} + [K(s) + K_{WT} + K_{mooring}]x \qquad (1)$$

where $M(s)$ is the platform structure mass matrix. $M(a)$ is the additional mass matrix. M_{WT} is the wind turbine mass matrix. $C(s)$ is the platform structure damping matrix. C_{WT} is the wind turbine damping matrix. $K(s)$ is the platform structure stiffness matrix. K_{WT} is the wind turbine stiffness matrix. $K_{mooring}$ is the mooring system stiffness matrix. $\ddot{x}$, $\dot{x}$, and x represent the acceleration vector, velocity, and displacement.
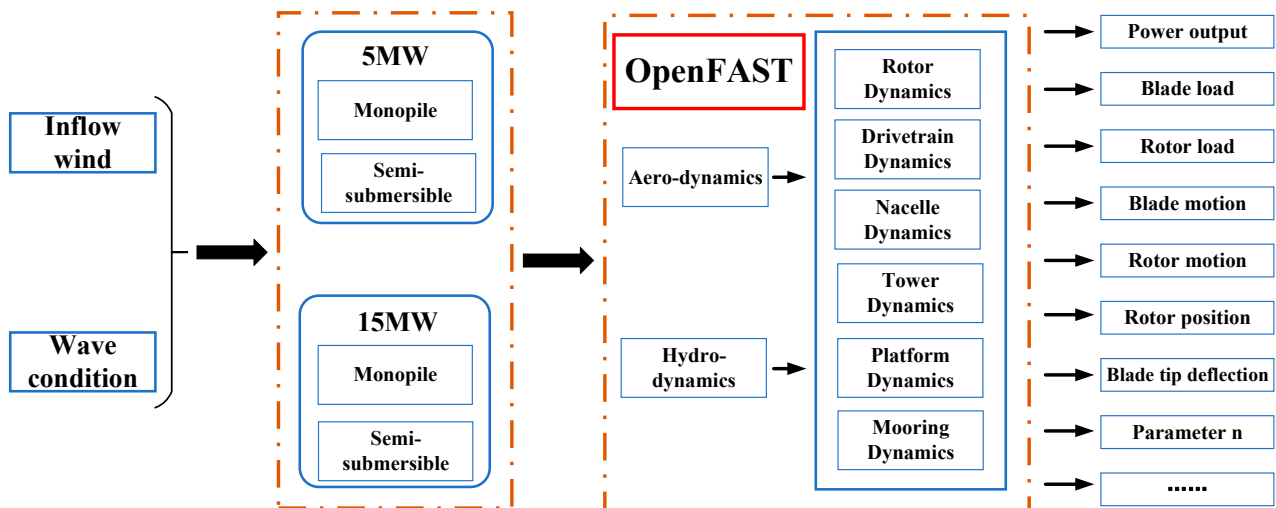

Figure 2. The diagram of the methodology.

2.2. Parameters of Wind Turbine and Semi Platform

The National Renewable Energy Laboratory (NREL) has established a 5 MW reference wind turbine, which is currently the most frequently used by researchers around the world [22]. The International Energy Agency (IEA) has developed a 15 MW wind turbine. At present, many researchers around the world are using this open-source wind turbine for analysis and study [23]. The NREL-5MW and IEA-15MW wind turbines have suitable semi-submersible foundations, so this study analyzes the NREL-5MW and IEA-15MW wind turbines.

2.2.1. NREL-5MW

The gross properties of the NREL-5MW reference wind turbine are shown in Table 1. The rotor radius of the 5 MW wind turbine is about 63 m. In order to enable the turbine to run at sea, the hub height of the reference wind turbine is set to 90 m, while the radius of the rotor remains unchanged and the hub height is as low as possible to reduce the overturning moment. When considering the extreme working conditions that occur once in 50 years, and the fact that the blade amplitude is 15 m, there is still an air gap of about 30 m between the adjacent blades. The actual NREL-5MW wind turbine uses blades with built-in pre-bending as a means of increasing the tower clearance without large rotor overhangs. Since many of the available simulation tools and design codes cannot support blades with pre-curves, we choose a 2.5° upwind pre-cone in the baseline wind turbine to represent the actual pre-cone amount. The basic parameters of the semi-type platform matching with the NREL-5MW are shown in Table 2. To ensure that the platform is stabilized, the semi-floating platform is moored with three catenary lines spread symmetrically about the platform Z-axis. The mooring line properties are listed in Table 3.

Table 1. Gross properties chosen for the NREL 5MW reference wind turbine.

Parameter	Value
Rating	5 MW
Rotor Orientation, Configuration	Upwind, 3 Blades
Control	Variable Speed, Collective Pitch
Drivetrain	High-Speed, Multiple-Stage Gearbox
Rotor, Hub Diameter	126 m, 3 m
Hub Height	90 m
Cut-In, Rated, Cut-Out Wind Speed	3 m/s, 11.4 m/s, 25 m/s
Cut-In, Rated Rotor Speed	6.9 rpm, 12.1 rpm
Rated Tip Speed	80 m/s
Overhang, Shaft Tilt, Pre-Cone	5 m, 5°, 2.5°
Rotor Mass	110,000 kg
Nacelle Mass	240,000 kg
Tower Mass	347,460 kg

Table 2. Semi-type floating platform geometry about NREL-5MW reference wind turbine.

Parameter	Value
Depth of platform base below SWL (total draft)	20 m
Elevation of main column (tower base) above SWL	10 m
Elevation of offset columns above SWL	12 m
Spacing between offset columns	50 m
Length of upper columns	26 m
Length of base columns	6 m
Depth to top of base columns below SWL	14 m
Diameter of main column	6.5 m
Diameter of offset (upper) columns	12 m
Diameter of base columns	24 m

Table 3. Mooring system properties about Semi-type NREL-5MW reference wind turbine.

Parameter	Value
Number of Mooring Lines	3
Angle Between Adjacent Lines	120°
Depth to Anchors Below SWL	200 m
Depth to Fairleads Below SWL	14 m
Radius to Anchors from Platform Centerline	837.6 m
Radius to Fairleads from Platform Centerline	40.868 m
Unstretched Mooring Line Length	835.5 m
Mooring Line Diameter	0.0766 m
Equivalent Mooring Line Mass Density	113.35 kg/m
Equivalent Mooring Line Mass in Water	108.63 kg/m
Equivalent Mooring Line Extensional Stiffness	753.6 MN
Hydrodynamic Drag Coefficient for Mooring Lines	1.1
Hydrodynamic Added-Mass Coefficient for Mooring Lines	1.0
Seabed Drag Coefficient For Mooring Lines	1.0
Structural Damping of Mooring Lines	2.0%

2.2.2. IEA-15MW

The NREL has released the International Energy Agency Wind Technology Collaboration Programme 15-megawatt reference turbine, or IEA Wind 15-MW, which features options for both bottom-fixed turbines and those with floating substructures. This open-source model can accommodate multiple software tools and provides industry, researchers, and academics with a public-domain tool for the design of next-generation offshore wind turbines.

Table 4 shows the gross parameters of the IEA-15MW reference wind turbine. The basic parameters of the semi-type platform matching with the IEA-15MW are shown in Table 5. The mooring system configuration consists of three 850-m-long chain catenary lines, and the mooring system properties and arrangement are provided in Table 6.

Table 4. Gross properties chosen for the IEA-15MW reference wind turbine.

Parameter	Value
Rating	15 MW
Rotor Orientation, Configuration	Upwind, 3 Blades
Control	Variable Speed, Collective Pitch
Drivetrain	Direct-Drive Configuration
Rotor, Hub Diameter	240 m, 7.94 m
Hub Height	150 m
Cut-In, Rated, Cut-Out Wind Speed	3 m/s, 10.95 m/s, 25 m/s
Minimum, Maximum Rotor Speed	5 rpm, 7.56 rpm
Rated Tip Speed	90 m/s
Shaft Tilt, Pre-Cone	6 deg, 4 deg
Blade Mass	65 t
Rotor Nacelle Assembly Mass	1017 t
Tower Mass	860 t

Table 5. Semi-type floating platform geometry about IEA-15MW reference wind turbine.

Parameter	Value
Platform Type	Semi-submersible
Freeboard	15 m
Draft	20 m
Total System Mass	20,093 t
Platform Mass	17,839 t
Tower Mass	1263 t
RNA Mass	991 t
Water Depth	200 m
Mooring System	Three-line chain catenary

Table 6. Mooring system properties about Semi-type IEA-15MW reference wind turbine.

Parameter	Value
Mooring System Type	Chain Catenary
Line Type	R3 Studless Mooring Chain
Line Breaking Strength	22,286 kN
Number of Lines	3
Anchor Depth	200 m
Fairlead Depth	14 m
Anchor Radial Spacing	8376 m
Fairlead Radial Spacing	58 m
Nominal Chain Diameter	185 mm
Dry Line Linear Density	685 kg/m
Extensional Stiffness	3270 MN
Line Unstretched Length	850 m
Fairlead Pretension	2437 kN
Fairlead Angle from SWL (Still Water Line)	56.4

3. Case Analysis

3.1. Inflow Wind

The wind condition is set to the normal turbulence model (NTM) and the Kaimal spectrum, the wind turbine level is IIB, and the corresponding reference turbulence intensity

under this level I_{ref} is 0.14; the sea shear coefficient α is also 0.14. The wind speed range is 9–13 m/s. The mean wind velocity profile varying with the height can be expressed as

$$U(z) = U_{hub} \left(\frac{z}{z_{hub}} \right)^{0.14} \tag{2}$$

where U_{hub} is the wind speed at the height of the hub; z_{hub} is the height of the hub center.

According to the Wind Energy Handbook [24], if no site is used to calculate the turbulence, the standard deviation of turbulence σ_1 can be estimated using the roughness parameter z_0. As shown in Equations (3) and (4), the turbulence intensity (TI) can be obtained from the turbulence standard deviation and the average wind speed at the height of the hub.

$$z_0 = \frac{A_c}{g} \left[\frac{k \cdot U_{hub}}{\ln(z_{hub}/z_0)} \right]^2 \tag{3}$$

$$TI = \frac{1}{\ln(z_{hub}/z_0)} + \frac{1.28 \times 1.44 \times I_{ref}}{U_{hub}} \tag{4}$$

where g is the acceleration of gravity; the unit is m/s^2. k is the von Karman constant; the value is 0.4. A_c is the Charnock constant; for the open sea, the value is 0.011. z_0 is the roughness parameter.

Figure 3 shows a schematic diagram of the change in the wind speed with time. In the series of simulations, three random seeds are adopted to produce a wind file in every environmental condition.
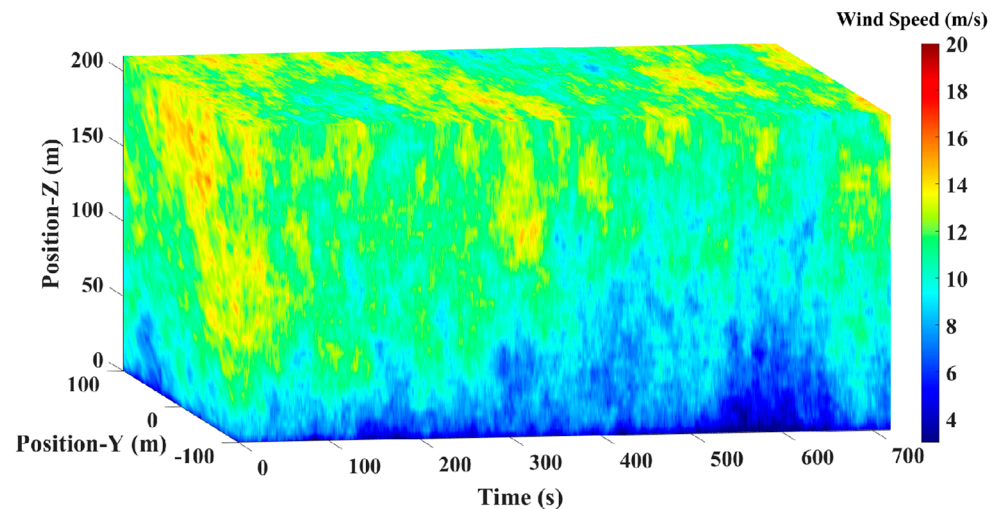

Figure 3. Schematic diagram of the change in wind speed with time.

3.2. Wave Condition

The NREL purchased 13-year wind and wave meteorological data from a reference station in Northeastern Scotland from BMT ARGOSS and analyzed them to obtain the relationship between the wave height H_s, peak period T_p, and U_{hub}, as shown in Figure 4 [25]. As the wind speed increases, the wave height and peak period also change. The first and second wave show a distinct difference in the motion and load of the floating wind turbine, and we only select the first-order wave for a more distinct and simple boundary condition. Based on this, this study selects the Pierson–Moskowitz spectrum to generate a single-directional wave along the turbines, but it does not consider a second-order wave force.
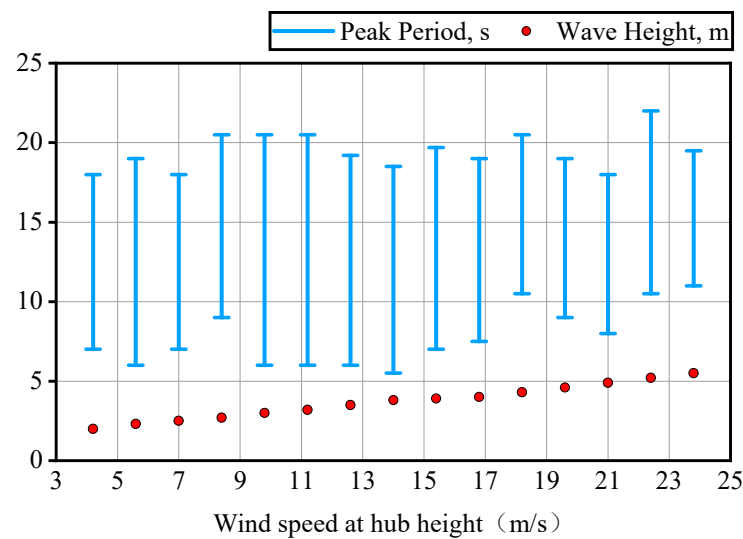
Figure 4. Statistical relationship between spectral peak period and wave height at different wind speeds.

3.3. Studied Cases

For all of the cases in Table 7, the wind and wave directions are aligned with the turbines. In order to ensure that the different cases have consistent wave conditions, we select the H_s of 2.9 m and the T_p of 12 s, combined with the selected wind speed in the cases presented in Figure 4. Every simulation runs for 1000 s, but we discard the initial 100 s period for more accurate results, because the wind turbine has not yet reached a stable working state at the beginning. The choice of the parameters seeks to minimize the calculation cost while ensuring the calculation accuracy.

Table 7. Case description.

Wind Speed	Turbulence Density	Wave Conditions	Wind and Wave Direction	Shear Coefficient
9–13 m/s, interval 1 m/s	Calculated by Formulas (4) and (5)	H_s is 2.9 m and T_p is 12 s	Aligned with the turbines	0.14

4. Results and Discussion

In this study, under environmental conditions of 8 m/s, 9 m/s, 10 m/s, 11 m/s, 12 m/s, and 13 m/s, a monopile (replaced by 5 M below) and semi foundation (replaced by 5 S in this study) for the NREL-5MW and a monopile-fixed foundation (replaced by 15 M in this study) and semi-floating foundation (replaced by 15 S in this study) for the IEA-15MW are analyzed and researched. As is known, the base of the bottom-fixed wind turbine is embedded in the seabed; the displacement of each component of the unit is only caused by the flexible deformation of the tower and other components, and the range is very small. In this study, the purpose of using a bottom-fixed turbine of the corresponding capacity is to perform a comparison so as to more intuitively determine the characteristics of the floating turbine.

According to the case conditions that we set, some time-varying parameters can be obtained. The rotor motion, blade motion, blade load, and power output are discussed in this section. From the intensity of the movement of the wind turbine, we can roughly determine the deformation of the blades. Then, the blade motion, including the blade tip motion and the clearance between the tower and blade, is analyzed. Following this, the load of the rotor and blade is shown. Finally, the power outputs for four types of wind turbines are studied.

4.1. Rotor Motion

Under the effect of wind and waves, as it has the highest altitude besides the blades, the movement range of the rotor largely reflects the intensity of the movement of the wind turbine.

In Figure 5, it can be clearly seen that the rotor movement range of the bottom-fixed turbine is very small compared to the floating unit, which can be regarded as indicating no displacement. With the increase in the wind speed, the displacement range of the rotor of the 5 S and 15 S cases shows an obvious increase. In the vicinity of the rated wind speed points corresponding to the 5 MW and 15 MW units, respectively, the displacement range of the wind rotor on the X-axis reaches the maximum value. When the wind speed is greater than the rated wind speed, the blade pitch angle changes, and the thrust that the wind turbine bears decreases; the displacement in the X-axis direction decreases accordingly. In the Y-axis direction, the displacement range of the wind rotor also tends to increase with the increase in the wind speed. One reason for this phenomenon is that the turbulence density changes with the wind speed. In the Z-axis direction, the position of the wind rotor is mainly related to the sea state. Since the water surface line area of the 5 S case is much smaller than that of the 15 S case, the wave has a significant impact on the 15 S case. The wave effect is more sensitive in the 15 S case, so the displacement range of the 15 S rotor on the Z axis is significantly larger than that of the 15 S case. After calculating the minimum cuboid volume that can enclose the displacement range of the rotor, it can be seen that, under the same environment, the displacement range of the 5 S rotor is much smaller than that of the 15 S case. The largest difference is at 11 m/s, and the rotor displacement of the 15 S case is 7.68 times than that of the 5 S case, which is 48.0374 m^3.

To summarize, near the rated wind speed, the displacement range of the rotor reaches a larger value. Before the rated wind speed, the displacement range of the rotor increases with the increase in the wind speed; after the rated wind speed, the displacement range of the rotor shows a downward trend.
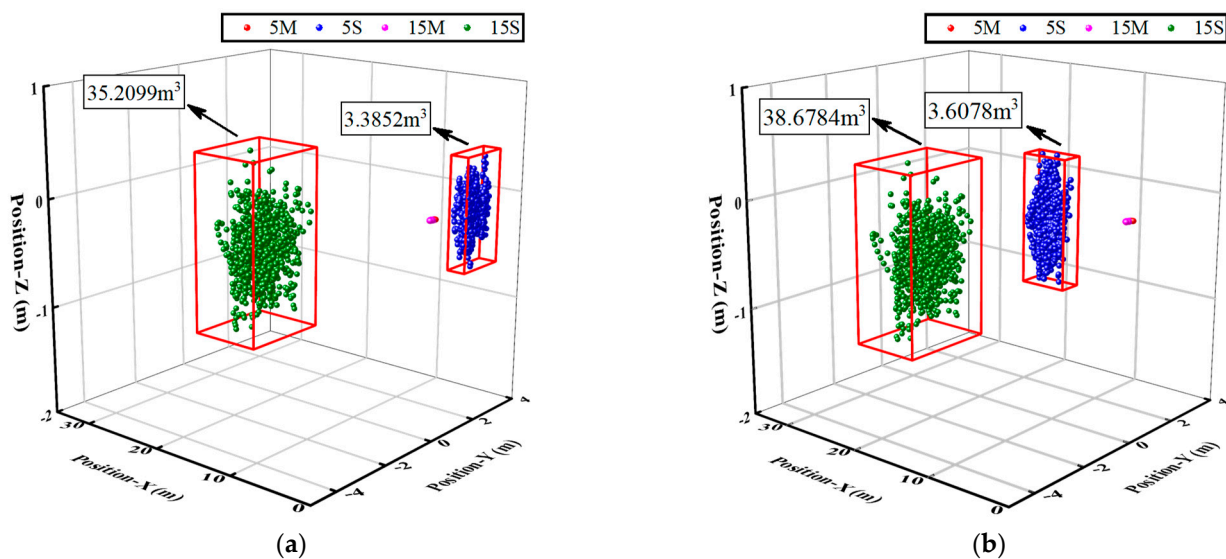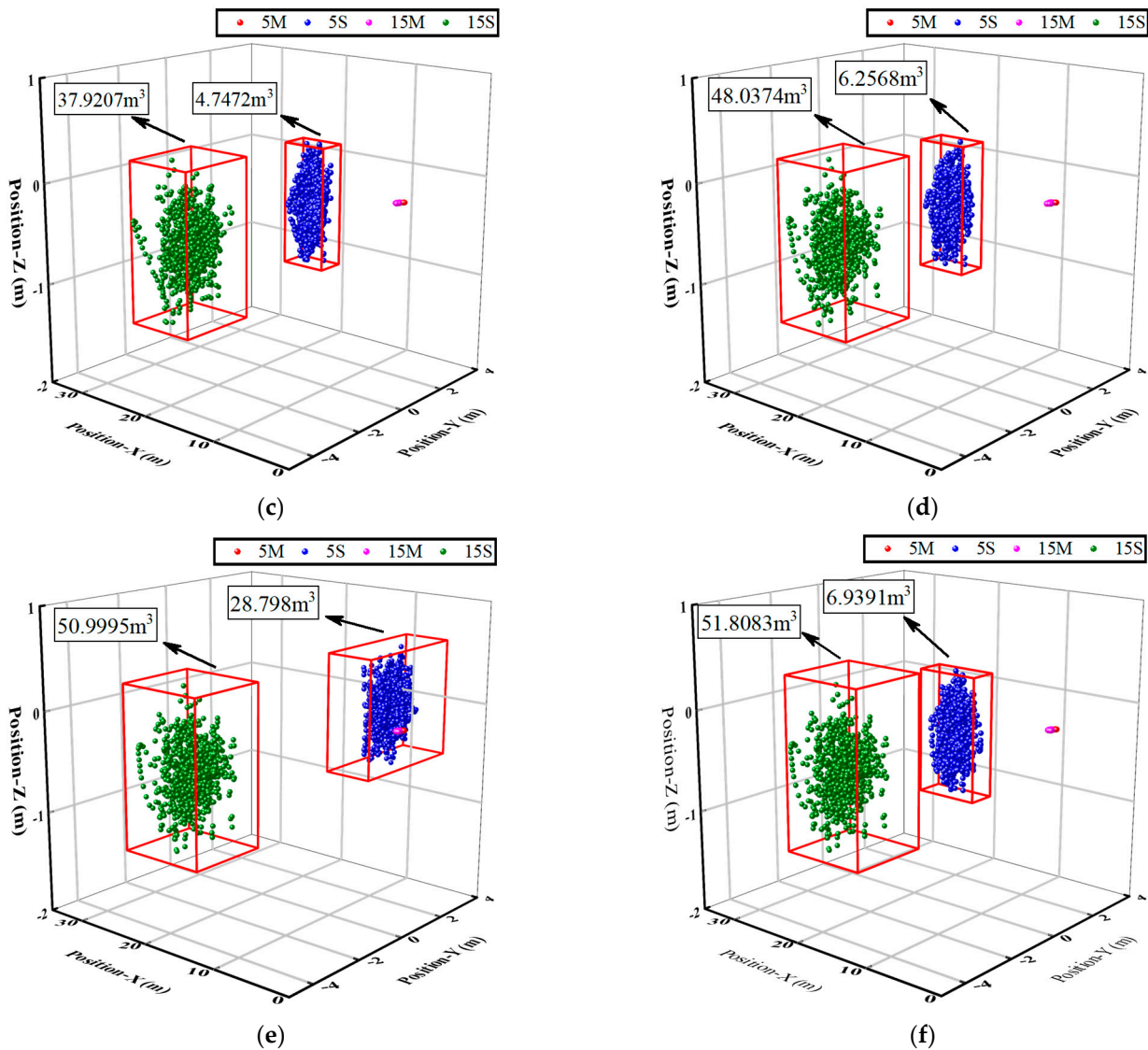

(a)

(b)

Figure 5. *Cont.*

(c)

(d)

(e)

(f)

Figure 5. Time series data of hub center position under wind speed of 8–13 m/s. (**a**) 8 m/s; (**b**) 9 m/s; (**c**) 10 m/s; (**d**) 11 m/s; (**e**) 12 m/s; (**f**) 13 m/s.

4.2. Blade Motion

4.2.1. Blade Tip Motion

The movement form of the blade can be divided into out-plane and in-plane types according to the rotation plane. The blade tip is the farthest end of the blade, and its movement range directly determines the safety and stability of the blade during operation.

It should be noted that the coordinate origin here is the intersection of the blade root and the rotating shaft, the X axis is the flow direction, the Z axis is the spanwise direction of the blade, and the coordinate system is rotated along with the blade. As shown in Figure 6, the blade tip movement range is outside of the rotated plane. Regardless of whether the wind turbines of the same capacity are installed on a bottom-fixed or semi-submersible foundation, the blade tip movement range and average value are essentially the same. However, because the bottom of the floating unit is not fixed, some of the movement of the blades is offset by the movement of the floating platform; thus, in most environments, the blade movement range of FOWTs is smaller. Under the same external environment, the blade tip swing amplitude of the IEA-15MW wind turbine is significantly larger than that of the NREL-5MW. The reason is that the blade length of the 15 MW wind turbine is nearly twice that of the 5 MW turbine, and the deformation of the blade is larger. It can

also be seen from the figure that the maximum blade tip swing amplitude of the 5 MW unit occurs at 11 m/s, while the maximum blade tip swing amplitude of the 15 MW unit occurs at 10 m/s. This is because the rated wind speed of the 5 MW unit is higher by about 1 m/s than that of the 15 MW unit. When the wind speed exceeds the rated wind speed, the pitch angle of the unit changes, the force on the blade changes, and the blade tip swing amplitude decreases accordingly.
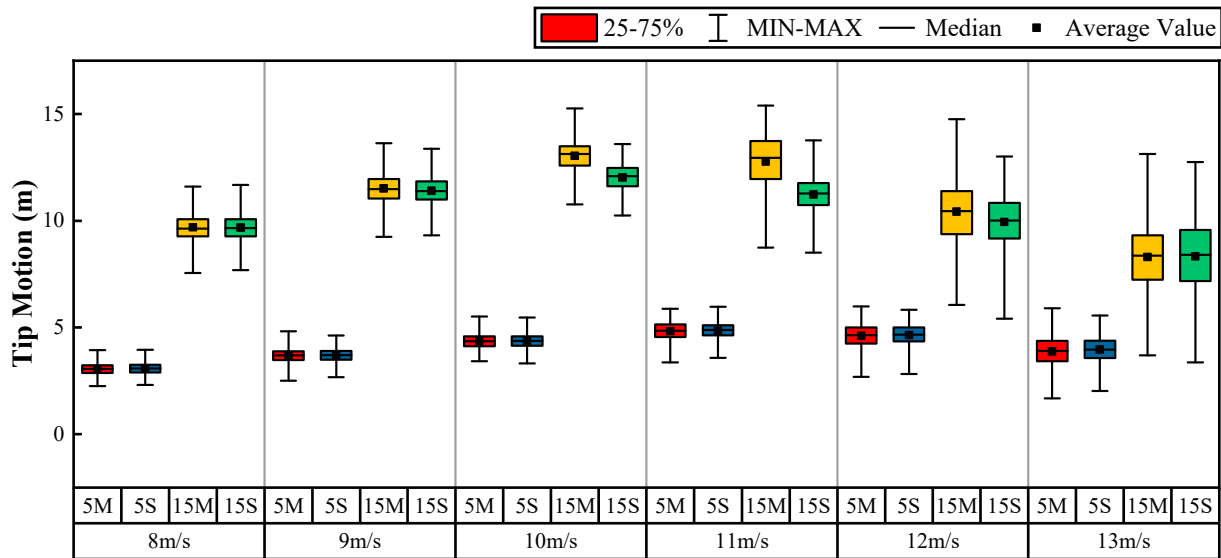

Figure 6. Blade 1 out-of-plane tip deflection.

The waving motion of the blade tip is motion in the plane of rotation, and the waving motion of the blade causes unstable loads at the blade root and fluctuations in the power output of the generator. Figure 7 shows a boxplot of the blade tip waving motion of the four types of turbines under various conditions. It can be clearly seen that the blade tip swing range and average value of the 5 M and 5 S units are essentially the same; the blade tip swing range and average value of the 15 M and 15 S units are also essentially the same. However, the waving motion range of the blade tip of the 15 MW unit is significantly larger than that of the 5 MW unit, while the average and median are similar. This is mainly due to the longer blade length of the large-capacity wind turbine and the greater flexible deformation of the blade. With the increase in the wind speed, the blade tip waving motion of the four types of units does not change significantly and remains essentially the same.
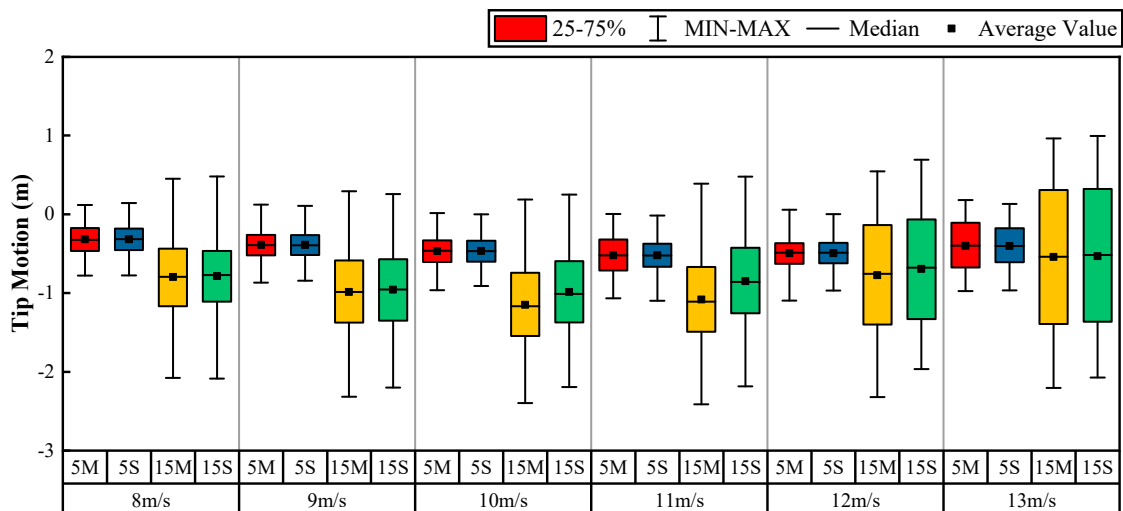

Figure 7. Blade 1 in-plane tip deflection.

4.2.2. Clearance between Tower and Blade

During operation, blade deformation will occur after receiving the thrust of the wind. This deformation will reduce the gap between the blade and the tower, resulting in a potential safety hazard. Therefore, it is necessary to analyze the clearance between the blade and the tower. In this section, a total of nine nodes of the blade are taken, and the average value of the clearance between these nine nodes and the tower within 101–1000 s is used, resulting in Figure 5. The distances of the blade nodes of the NREL-5MW unit from the blade root are (1.37 m, 6.83 m, 14.35 m, 22.55 m, 30.75 m, 38.95 m, 47.15 m, 54.67 m, 60.13 m), and the distances of the blade nodes of the IEA-15MW unit from the blade root are (9.55 m, 21.49 m, 33.43 m, 45.37 m, 57.31 m, 69.24 m, 81.18 m, 93.12 m, 105.06 m).

For the NREL-5MW wind turbine, whether it is installed on a monopile or a semi foundation, the gap difference between the blades and the tower is not obvious. When the wind speed is below the rated speed, the two curves almost overlap. This is mainly due to the limited length of the 5 MW blade and the small flexible deformation of the blade; although the platform is different, the gap between the blade and tower is also small. At 11 m/s and 12 m/s, the air gap between the blade and tower is the smallest, and the bending degree of the blade is also the most obvious. At this time, the blade suffers the largest thrust. The distances between the ninth nodes in the 5 M and 5 S cases from the tower at these two wind speeds are 5.62 m, 5.81 m and 5.41 m, 5.48 m, respectively. For the IEA-15MW, the length of the blade is nearly 120 m, and the flexible deformation of the blade is very large. Therefore, if it is installed on a different platform, the gap between the blade and tower will be quite different. It can be seen from Figure 8a–f that, except at 8 m/s, the clearance between the blades and tower of the two platforms is not similar. Under other wind speeds, the clearance between the blades and the tower of the semi unit is greater than that for the monopile turbine, which is because the foundation of the semi unit is not fixed on the seabed. When the wind rotor is thrust and the unit is inclined, the water on the foundation can play a certain buffering role. Near the rated wind speed, the 15 MW units in the monopile and semi configurations have the largest difference in the blade–tower clearance and the smallest blade–tower clearance for the two types of platforms. At 10 m/s, the gap between the ninth node of the monopile unit and the tower is 18.26 m, and the distance of the semi type is 19.62 m.
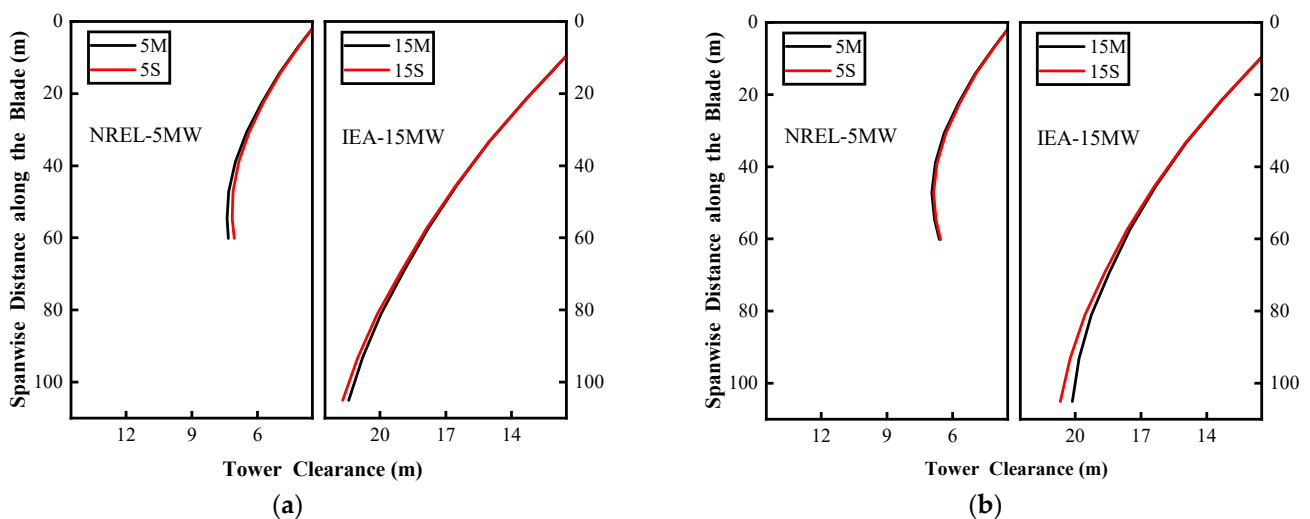

Figure 8. *Cont.*
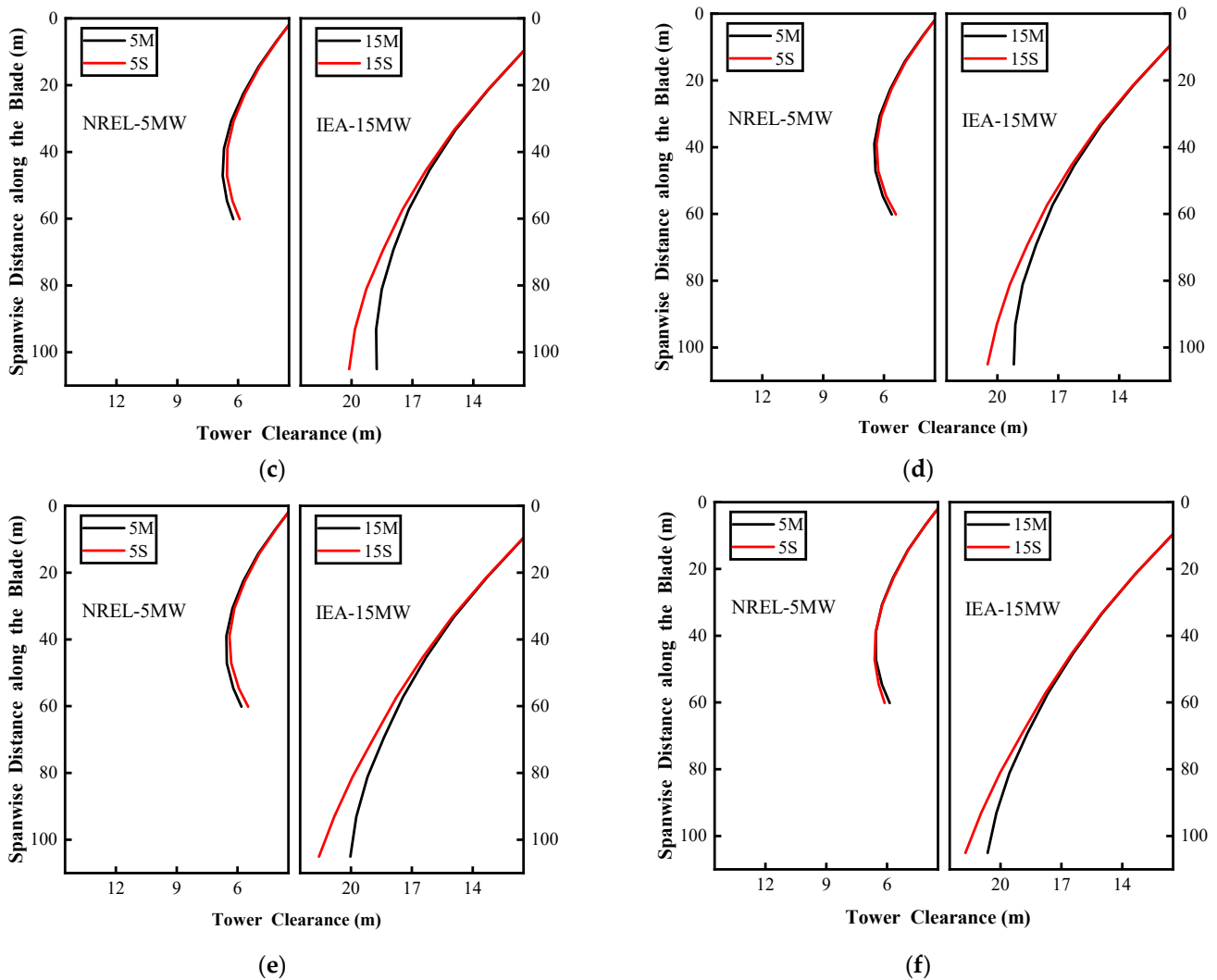
(c)

(d)

(e)

(f)

Figure 8. The average value of the minimum clearance between each node of the blades and the tower for the NREL-5MW and IEA-15MW wind turbines under the wind speed of 8–13 m/s. (**a**) 8 m/s; (**b**) 9 m/s; (**c**) 10 m/s; (**d**) 11 m/s; (**e**) 12 m/s; (**f**) 13 m/s.

4.3. Blade Load

4.3.1. Axial Load of Rotor

The load of the rotor in the inflow wind direction directly reflects the blade load. As shown in Figure 9, under the wind speed of 8–13 m/s, the load on the rotor in the 5 M and 5 S cases is essentially the same. At 11 m/s, the load of both the 5 M and 5 S rotors reaches the maximum value. The rotor of 5 M suffers a load of 613.4 kN and the 5 S receives a load of 608.2 kN, and the difference is only 5.2 kN. The maximum force on the 15 M and 15 S rotors occurs at 10 m/s and 11 m/s. At this time, the rotor load of the 15 M case is 1952.3 kN and the load of the 15 S case is only 89.09% of that of the 15 M case, and the value is 1739.3 kN. Regarding the difference between the fixed type and the semi-submersible type, it is obvious that the large-capacity wind turbine has a greater difference. The reason for this phenomenon is that the swept area of the wind turbine increases with the square of the blade length, and the thrust received by the rotor is proportional to the swept area of the rotor.
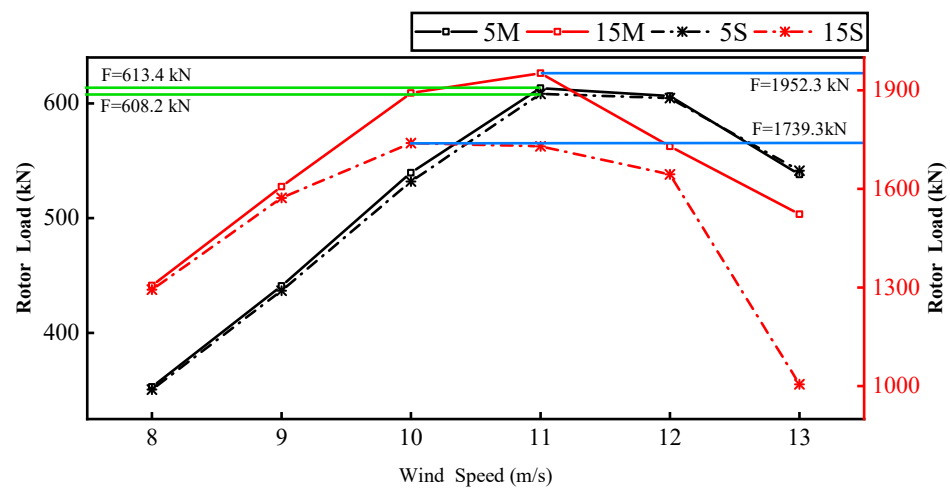
Figure 9. The wind load on the rotor in the X-axis direction.

4.3.2. Blade Root Load

As shown in Figure 10, the maximum blade root load of both the 5 MW and 15 MW wind turbines occurs near the rated wind speed. At this time, the blade pitch angle either does not act or has recently started to act. Because the 15 MW wind turbine has a large sweeping area, the thrust that it receives is many times that of the 5 MW wind turbine, so the load at its blade root is also much larger than that of the 5 MW wind turbine. From the perspective of a wind speed of 8–13 m/s, in most working conditions, the difference in the blade root load of the 15 MW wind turbines installed on monopile and semi foundations is larger than that of the 5 MW unit (it should be noted that the Y-axis coordinate range of Figure 10a is not consistent with that of Figure 10b). At 13 m/s, the blade root load difference between 5 M and 5 S reaches the maximum value of 9.4 kN; similarly, at 11 m/s, the blade root load difference between the 15 M and 15 S wind turbines also reaches the maximum value of 35.7 kN. From the perspective of the change in the pitch angle, the difference between the 15 MW units installed on the fixed and floating foundations is also larger, which is mainly due to the larger linear speed of the large-capacity unit when shaking, which causes the relative wind speed of the 15 MW unit to be larger and the rated wind speed of the 15 MW unit to be lower. This makes it easier for the relative wind speed to reach the rated wind speed of the 15 MW turbine, resulting in more frequent pitch angle actions.
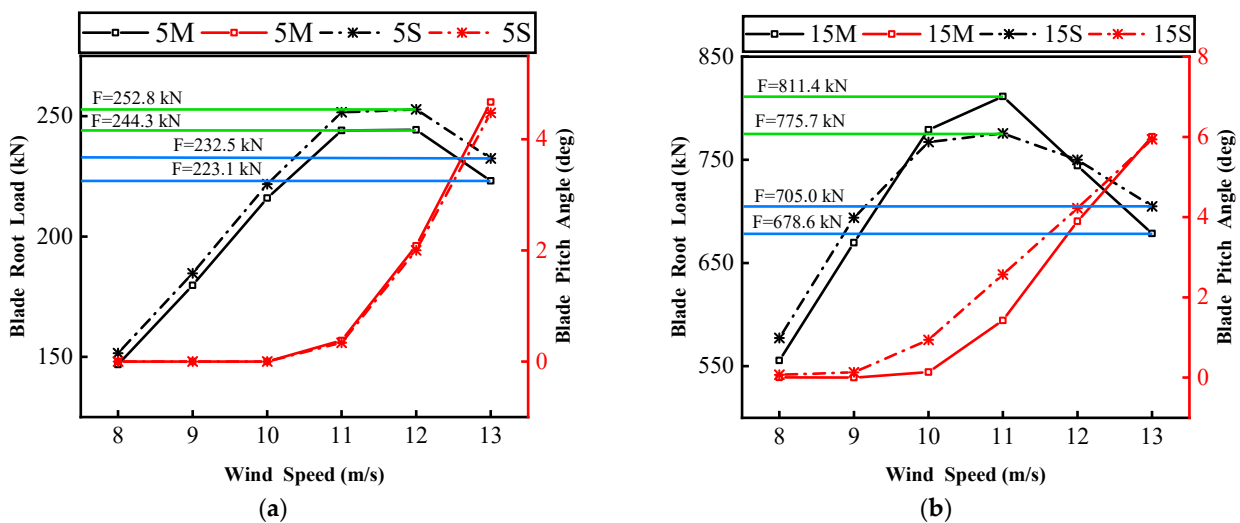

(a)

(b)

Figure 10. Relationship between blade root load and pitch angle of NREL-5MW and IEA-15MW units. (**a**) NREL-5MW; (**b**) IEA-15MW.

4.4. Power Output

Factors such as the movement of the rotor and the flexible deformation of the blades will cause fluctuations in the power output and a reduction in the total power output. Figure 11 shows the power output time series data of the 5 M, 5 S and 15 M, 15 S cases from 101 to 1000 s at wind speeds of 8 m/s, 10 m/s, and 13 m/s, respectively. When the wind speed is lower than the rated wind speed, the power curves of the 5 M and 5 S cases have a obvious difference, but the power fluctuation for 5 S is obvious, and the curve has a sawtooth pattern. When the wind speed is higher than the rated wind speed, the power fluctuation of the 5 S turbine is large and frequent. For the 15 MW turbine, it can be clearly seen that the power fluctuation of the 15 S unit is very obvious, and most of the power curves of the 15 S unit are below 15 M. For floating wind turbines, the main reason for the fluctuation in power is the movement of the wind rotor in the direction of the inflow wind, so that the relative wind speed faced by the wind rotor is the ambient wind speed plus the movement speed of the wind rotor. A very important reason for the low power output of FOWTs is that floating wind turbines will tilt, thereby reducing the sweeping area of the rotor, which is especially obvious when the wind speed is lower than the rated wind speed.
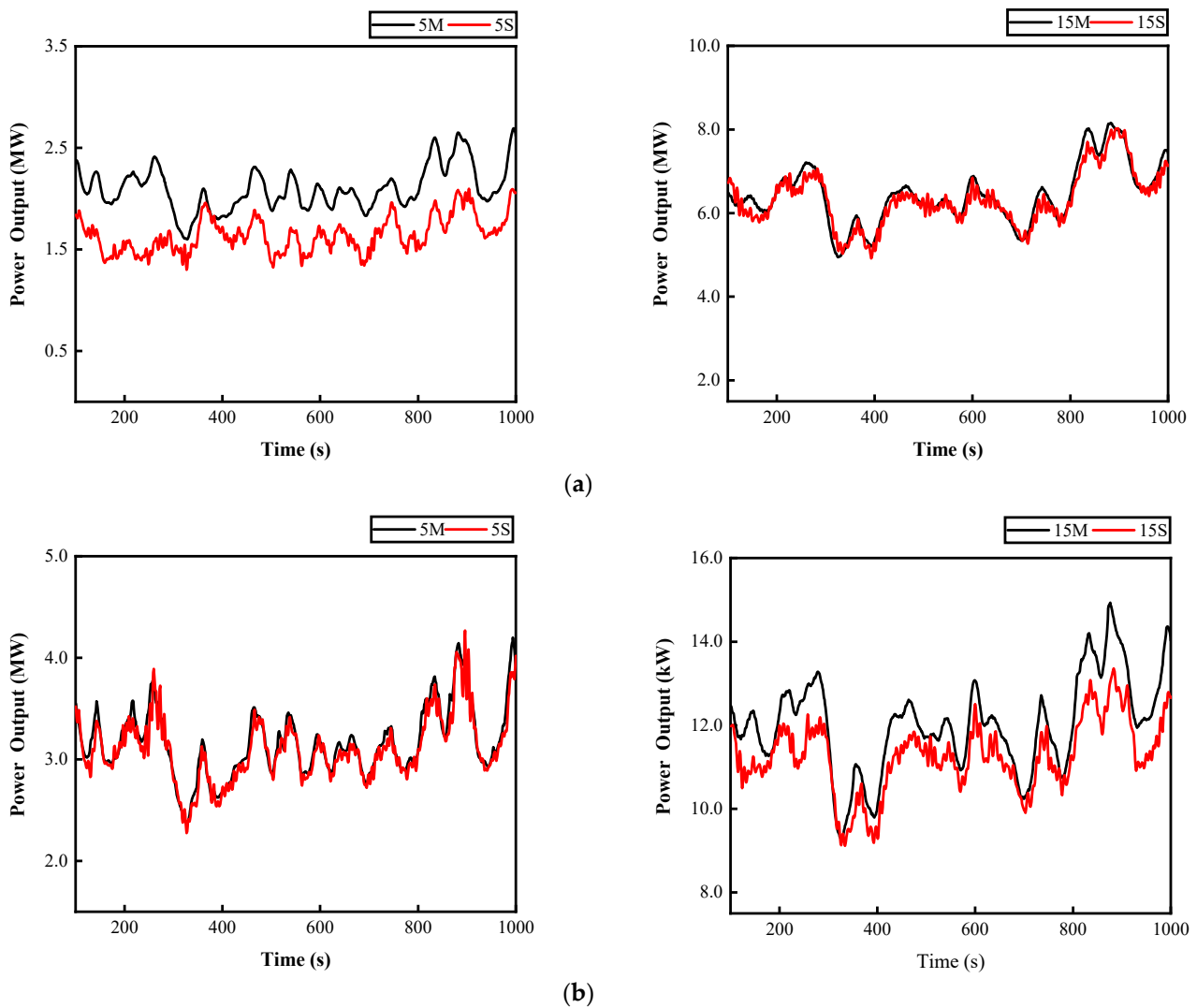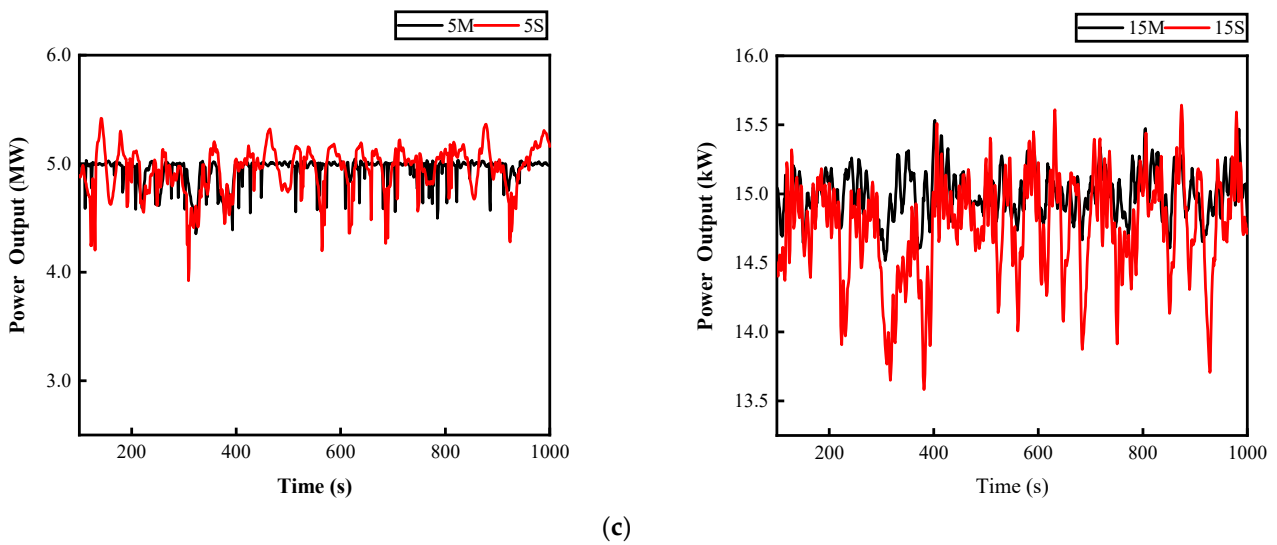

(**a**)

(**b**)

Figure 11. *Cont.*

(**c**)

Figure 11. Time series data of power output at wind speed of 8–13 m/s. (**a**) 8 m/s; (**b**) 10 m/s; (**c**) 13 m/s.

It can also be clearly seen from Figure 12 that, when comparing the monopile and semi wind turbines in the same environment, the semi wind turbine has a lower power output than the monopile type. As the capacity increases, the difference in the power output between the bottom-fixed and floating turbines is more obvious; the most obvious difference in the power output occurs near the rated wind speed, because, at this time, the rotor receives the greatest thrust and the degree of inclination is also the most severe. As shown in Table 8, the quantified power output can be obtained. When the wind speed is at 10 m/s, the largest difference between 5 M and 5 S occurs, and the 5 M's power output is 101.93 percent of that of 5 S; the difference is 60.02 kW. At 11 m/s, the largest difference between 15 M and 15 S is produced, and the 15 M's power output is 109.17 percent of that of 15 S; the difference is 1203.79 kW, which represents high power production for a wind turbine.
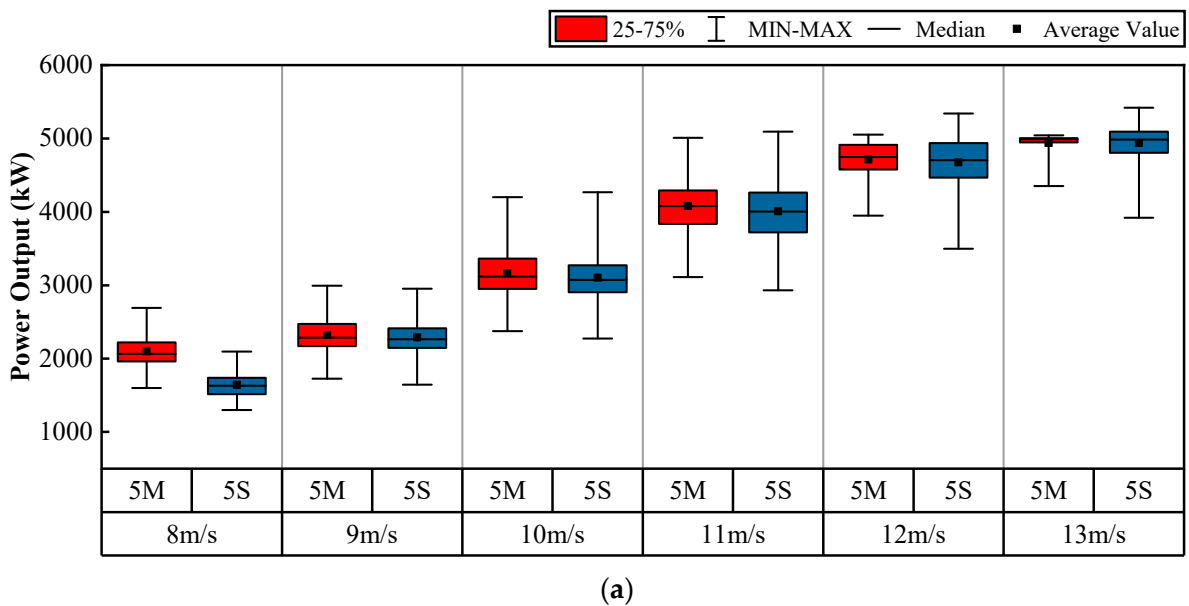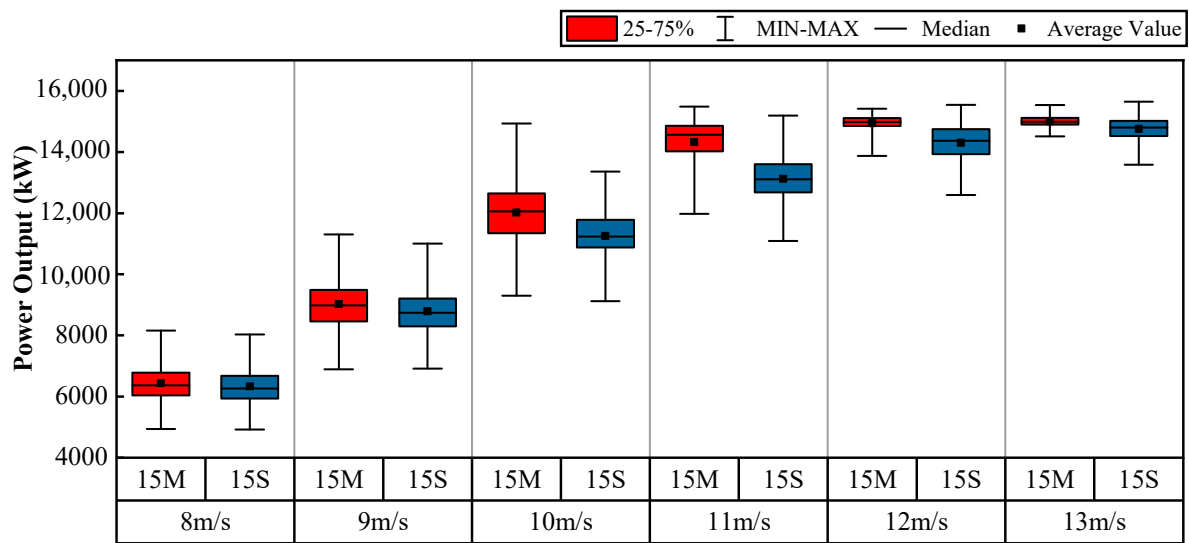

(**a**)

Figure 12. *Cont*.

Figure 12. Power output of NREL-5MW and IEA-15MW at 8–13 m/s wind speed. (**a**) NREL-5MW; (**b**) IEA-15MW.

Table 8. The quantification of the total average power output for four types of wind turbines at 8–13 m/s.

Wind Speed	Average Power Output of 5 M	Average Power Output of 5 S	Value of 5 M/5 S	Average Power Output of 15 M	Average Power Output of 15 S	Value of 15 M/15 S
8 m/s	1639.73 kW	1622.90 kW	101.04%	6437.30 kW	6334.08 kW	101.63%
9 m/s	2321.79 kW	2288.64 kW	101.45%	9022.90 kW	8785.83 kW	102.70%
10 m/s	3162.04 kW	3102.02 kW	101.93%	12,019.21 kW	11,257.58 kW	106.77%
11 m/s	4079.20 kW	4006.48 kW	101.82%	14,325.45 kW	13,121.66 kW	109.17%
12 m/s	4713.35 kW	4674.16 kW	100.84%	14,939.11 kW	14,302.53 kW	104.45%
13 m/s	4939.21 kW	4938.22 kW	100.02%	15,002.25 kW	14,752.85 kW	101.69%

5. Conclusions

For FOWTs, the blade's motion and load characteristics and the fluctuations in the power output show a distinct difference from those of a bottom-fixed wind turbine, even in the same external environment, due to the additional DoFs. If we analyze the blade characteristics and power output of FOWTs individually, without the bottom-fixed wind turbine as a comparison, we cannot obtain an intuitive understanding of the FOWTs' data. Thus, this study adopts the most used floating platform—the semi—and a monopile-type bottom-fixed wind turbine for simulations and calculations. Moreover, the differences between the large-capacity FOWT and its corresponding bottom-fixed wind turbine show significant variance compared to the small-capacity wind turbine, so we select two types of wind turbines with different capacities, the NREL-5MW and IEA-15MW, to carry out comparative studies.

In the present study, we select and set the parameters of the wind turbines, as well as their foundations, for the studied cases, including the wind conditions, wave conditions, and case settings. Then, simulations are run using OpenFAST and the results are discussed using various types of plots. The following conclusions are obtained.

The movement range of the rotor of the FOWT is much larger than that of the bottom-fixed wind turbine. As the capacity of the turbine increases, the displacement range of the wind rotor increases, which is mainly because the diameter of the rotor and the height of the hub center also increase with the increase in the unit capacity. The largest difference is at 11 m/s, and the rotor displacement of the 15 S case is 7.68 times that of the 5 S case, which is 48.0374 m^3.

There is no significant difference in the blade tip out-of-plane deflection between the FOWT and bottom-fixed wind turbine with a small capacity. For the large-capacity wind turbine, the FOWT's blade tip out-of-plane deflection is lower than that of the monopile-type wind turbine. Regarding the clearance between each node of the blades and the tower, we obtain the same conclusion. Thus, the 15 M's clearance is the smallest, especially near the rated wind speeds. When the wind speed is at 10 m/s, the 15 M's clearance shows the lowest value, and the gap between the ninth node of the monopile unit and the tower is 18.26 m; the distance for the semi type is 19.62 m.

The power fluctuations of FOWTs are significantly larger than those of bottom-fixed wind turbines. Since FOWTs will tilt when subjected to wind loads, the power output is lower than in bottom-fixed wind turbines. As the capacity of the unit increases, the difference in the power outputs of floating and fixed units is larger, and the greatest difference generally occurs near the rated wind speed. At 11 m/s, the largest difference between the 15 M and 15 S cases is produced, and the 15 M's power output is 109.17 percent of that of 15 S; the difference is 1203.79 kW, which represents high power production for a wind turbine.

Through the analysis presented in this article, researchers can obtain a more intuitive understanding of the blade characteristics and power output fluctuations of semi-submersible FOWTs. It provides a certain reference for the future structural design and control system design of semi-submersible wind turbines.

Author Contributions: Conceptualization, J.C. and Z.C.; methodology, J.C. and P.L.; Software, J.C. and R.M.; formal analysis, J.C. and H.P.; investigation, J.C. and R.M.; resources, Z.C. and P.L.; writing—original draft preparation, J.C.; writing—review and editing, Y.L., Q.L. and R.M.; project administration, P.L.; funding acquisition, R.M. and Q.L. All authors have read and agreed to the published version of the manuscript.

Data Availability Statement: Due to the large volume of data, they cannot be shared via a network drive. To access them, the author can be contacted at cuijiaping2024@163.com. The key data can be provided due to their smaller volume.

Conflicts of Interest: Authors Zhigang Cao and Pin Lyu were employed by the Goldwind Science & Technology Co., Ltd. Authors Huaiwu Peng was employed by the Power China Northwest Engineering Co., Ltd. The remaining authors declare that the research was conducted in the absence of any commercial or financial relationships that could be construed as a potential conflict of interest.

References

1. Veers, P.; Dykes, K.; Lantz, E.; Barth, S.; Bottasso, C.L.; Carlson, O.; Clifton, A.; Green, J.; Green, P.; Holttinen, H.; et al. Grand challenges in the science of wind energy. *Science* **2019**, *366*, eaau2027. [CrossRef] [PubMed]
2. Greco, L.; Testa, C. Wind turbine unsteady aerodynamics and performance by a free-wake panel method. *Renew. Energy* **2021**, *164*, 444–459. [CrossRef]
3. Zhao, Z.; Shi, W.; Wang, W.; Qi, S.; Li, X. Dynamic analysis of a novel semi-submersible platform for a 10 MW wind turbine in intermediate water depth. *Ocean. Eng.* **2021**, *237*, 109688. [CrossRef]
4. Bai, H.; Zhang, M.; Yuan, W.; Xu, K. Conceptual design, parameter optimization and performance investigation of a 10 MW semi-submersible floating wind turbine in shallow water. *Ocean. Eng.* **2023**, *281*, 114895. [CrossRef]
5. Zhang, H.; Zhang, N.; Cao, X. Conceptualization and dynamic response of an integrated system with a semi-submersible floating wind turbine and two types of wave energy converters. *Ocean. Eng.* **2023**, *269*, 113517. [CrossRef]
6. Shen, X.; Chen, J.; Hu, P.; Zhu, X.; Du, Z. Study of the unsteady aerodynamics of floating wind turbines. *Energy* **2018**, *145*, 793–809. [CrossRef]
7. Roh, C.; Ha, Y.J.; Ahn, H.J.; Kim, K.-H. A Comparative Analysis of the Characteristics of Platform Motion of a Floating Offshore Wind Turbine Based on Pitch Controllers. *Energies* **2022**, *15*, 716. [CrossRef]
8. Lienard, C.; Boisard, R.; Daudin, C. Aerodynamic behavior of a floating offshore wind turbine. *AIAA J.* **2020**, *58*, 3835–3847. [CrossRef]

9. Kim, K. Effect of Platform Motion on Aerodynamic Performance and Aeroelastic Behavior of Floating Offshore Wind Turbine Blades. *Energies* **2019**, *12*, 2519. [CrossRef]
10. Dai, J.; Hu, W.; Shen, X. Load and dynamic characteristic analysis of wind turbine flexible blades. *J. Mech. Sci. Technol.* **2017**, *31*, 1569–1580. [CrossRef]
11. Bozzo, A. Dynamic Analysis of Floating Offshore Wind Turbines under Extreme Operational Conditions (Order No. 30423233). Master's Thesis, University of New Hampshire, Durham, NH, USA, 2023.
12. Yu, Z.; Ma, Q.; Zheng, X.; Liao, K.; Sun, H.; Khayyer, A. A hybrid numerical model for simulating aero-elastic-hydro-mooring-wake dynamic responses of floating offshore wind turbine. *Ocean. Eng.* **2023**, *268*, 113050. [CrossRef]
13. Liang, G.; Lopez-Olocco, T.; Medina-Manuel, A.; Saavedra-Ynocente, L.A.; Souto-Iglesias, A.; Jiang, Z. Experimental investigation of two shared mooring configurations for a dual-spar floating offshore wind farm in irregular waves. *Mar. Struct.* **2024**, *95*, 103579. [CrossRef]
14. Wang, K.; Gaidai, O.; Wang, F.; Xu, X.; Zhang, T.; Deng, H. Artificial Neural Network-Based Prediction of the Extreme Response of Floating Offshore Wind Turbines under Operating Conditions. *J. Mar. Sci. Eng.* **2023**, *11*, 1807. [CrossRef]
15. Robertson, A.; Jonkman, J.; Masciola, M.; Song, H.; Goupee, A.; Coulling, A.; Luan, C. *Definition of the Semisubmersible Floating System for Phase II of OC4*; Scitech Connect Definition of the Floating System for Phase IV of OC3; National Renewable Energy Laboratory: Golden, CO, USA, 2014.
16. Jonkman, J. *Definition of the Floating System for Phase IV of OC3*; Scitech Connect Definition of the Floating System for Phase IV of OC3; National Renewable Energy Laboratory: Golden, CO, USA, 2010.
17. Matha, D.; Fischer, T.; Kuhn, M.; Jonkman, J. *Model Development and Loads Analysis of a Wind Turbine on a Floating Offshore Tension Leg Platform*; National Renewable Energy Laboratory: Golden, CO, USA, 2010.
18. Shi, W.; Zhang, L.; Karimirad, M.; Michailides, C.; Jiang, Z.; Li, X. Combined effects of aerodynamic and second-order hydrodynamic loads for floating wind turbines at different water depths. *Appl. Ocean. Res.* **2023**, *130*, 103416. [CrossRef]
19. Kara, F. Coupled dynamic analysis of horizontal axis floating offshore wind turbines with a spar buoy floater. *Wind. Eng.* **2023**, *47*, 607–626. [CrossRef]
20. Javier López-Queija Robles, E.; Llorente, J.I.; Touzon, I.; López-Mendia, J. A Simplified Modeling Approach of Floating Offshore Wind Turbines for Dynamic Simulations. *Energies* **2022**, *15*, 2228. [CrossRef]
21. Jonkman, J.M.; Buhl, M.L. *FAST User's Guide*; National Renewable Energy Laboratory: Golden, CO, USA, 2005.
22. Jonkman, J.M.; Butterfield, S.; Musial, W.; Scott, G. *Definition of a 5 MW Reference Wind Turbine for Offshore System Development*; Office of Scientific & Technical Information Technical Reports; National Renewable Energy Laboratory: Golden, CO, USA, 2009.
23. Gaertner, E.; Rinker, J.; Sethuraman, L.; Zahle, F.; Anderson, B.; Barter, G.; Abbas, N.; Meng, F.; Bortolotti, P.; Skrzypinski, W.; et al. *IEA Wind TCP Task 37: Definition of the IEA Wind 15-Megawatt Offshore Reference Wind Turbine (Technical Report)*; National Renewable Energy Laboratory: Golden, CO, USA, 2020; NREL/TP-5000-75698.
24. Burton, T. *Wind Energy Handbook*; Wiley: Hoboken, NJ, USA, 2011.
25. Robertson, A.N.; Jonkman, J.M. Loads analysis of several offshore floating wind turbine concepts. In Proceedings of the ISOPE International Ocean and Polar Engineering Conference, Maui, HI, USA, 19–24 June 2011; ISOPE-I-11-204.